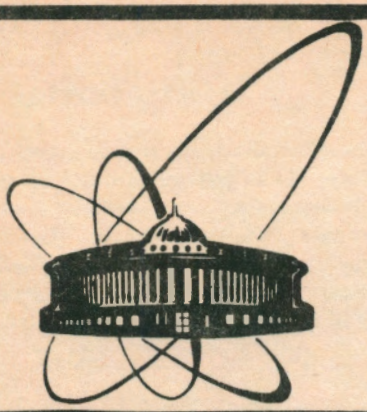

сообщения
объединенного
института
ядерных
исследований
дубна

E4-92-458

F.A.Gareev, S.N.Ershov, G.S.Kazacha, E.F.Svinareva,
S.Yu.Shmakov, V.V.Uzhinski

STUDY OF PROPERTIES OF EXOTIC NUCLEI USING ELASTIC SCATTERING. THEORETICAL CONSIDERATION

1992

1 Introduction

Historically, nuclear physicists preferred projectiles that were as simple as possible, the focus was only on one of the reaction partners, the target. This attitude was obviously also linked to a limited ability to produce qualitative beams of heavier nuclei in the early light-ion era. With the heavy-ions a more democratic treatment of the two reaction partners became a necessity and focus has been shifted to the projectile with the occurrence of exotic radioactive beams.

With increased ambitions for a quantitative understanding of quasielastic reactions, such as charge-exchange or nucleon-transfer, a qualitative description of the projectile-ejectile partners of the collision is also called for. One hopes that the very nature of exotic beams will enhance fundamental aspects of such reactions and thus will serve as an extreme testing ground. The reduced intensity of such beams obviously does not make the job easy.

The recent progress in the light radioactive beam technique provides unique possibilities to study the nuclear structure near the neutron drip line. The ^{11}Li nucleus is partially interesting, the existence of a neutron halo having been experimentally proved. Apparently, the ^{6}He nucleus is another candidate for a neutron halo nucleus which has properties similar to ^{11}Li (abnormally large electromagnetic dissociation cross section, a very large radius in the nuclear scale, twofold component momentum distribution of α-particles for fragmentation of ^{6}He on light targets [1]).

The experimental studies of the $^{11}Li+p$ [2] and $^{11}Li+^{28}Si$ [3] elastic scattering are in the very beginning, experiments of the $^{6}He+p$ elastic scattering are also in progress. These studies will certainly probe the extension of the halo, but being a highly integrated (inclusive) observable, elastic scattering may not carry much information on the detailed halo-structure of the exotic nuclei such as ^{11}Li, reaction processes (for example, two-neutron transfer reactions $p(^{11}Li,^{9}Li)t$ or $^{12}C(^{11}Li,^{9}Li)^{14}C$ [4]) being better candidates. Discussions of the latter made, however, in standard theoretical approaches rely on elastic channel information for their optical potentials. The main ingredient in the conventional treatment of elastic scattering is the single particle densities evaluated in some nuclear models.

Details of the ^{11}Li density are still somewhat a matter of debate. The situation is more clear-cut for ^{6}He, also a halo-like nucleus. Contrary to ^{11}Li the existing experimental data for N-N and N-α scattering allow us to extract the corresponding potentials and hence we can calculate reasonably correct wave functions for the system $N+N+\alpha$ in the framework of the microscopic three-body approach [5]. In ref. [6] the calculated wave functions and corresponding densities were tested against a variety of weak and electromagnetic data as well as nucleon- induced quasielastic reactions (p,p'), (n,p) and (p,n) on ^{6}Li as a target. An additional possibility to test the resulting wave functions is to compare ^{6}Li and ^{6}He elastic scattering on proton and nucleus targets; the structures of these nuclei are comparable in a global sense (in the framework of a three-body model) but differ in the correlations of the extra nucleons which may be examined experimentally. Therefore, we carry out a comparative analysis of elastic scattering of ^{6}Li and ^{6}He, ^{11}Li and ^{12}C on proton and nucleus targets at intermediate energies within the framework of the optical potential model and Glauber approach.

The main aim of this paper is to describe the theoretical procedure and to discuss the effect of the halo-like structure of ^6He and ^{11}Li on elastic scattering.

2 Optical model analysis of ^{11}Li elastic scattering on ^{28}Si at E/A=29 MeV

To elucidate the behavior of interaction potentials for exotic nuclei, recent data from elastic scattering of secondary ^{11}Li (29 MeV/A) and ^7Li (25.4 MeV/A) beams on ^{28}Si measured at Ganil [7] (Ganil-Dubna collaboration) are useful. The corresponding angular distribution for ^7Li is shown in Fig.1. It is in qualitative agreement with measurements at lower projectile energies [8]. All they have shapes typical of stable nuclei scattering in the Fraunhofer diffraction region - the ratio σ/σ_R decreases with increasing scattering angle. The use of the thick target, the angular resolution $\delta\theta \approx 1.5°$ and the lack of separation between elastic and inelastic scattering results in a flattening of the diffraction structure of the spectra in Fig.1. For the case of ^{11}Li (Fig.2.) the behavior of experimental data is unusual - the ratio σ/σ_R is almost constant in the measured range of angles. or has some tendency to decrease with increasing scattering angle. Furthermore, σ/σ_R exceeds for ^{11}Li the one observed in an analogous distribution for the elastic scattering of the loosely bound nuclei ^6Li [9] and ^9Be [10] on ^{28}Si at approximately the same energies of relative motion.

The analysis of the elastic scattering was carried out in the framework of the conventional optical model using the standard Saxon-Woods form,

$$U(r) = V_{Coul}(r) - Vf(x_R) - iWf(x_I),$$

$$f(x_i) = (1 + exp[(r - R_i)/a_i])^{-1},$$

where $R_i = r_i A_T^{1/3}$ while $V_{Coul}(r)$ is the Coulomb potential of the uniformly charged sphere. Potential parameters were fitted by the χ^2 method for the best description of the experimental data.

We estimated the inelastic cross section in the framework of the DWBA, with an inelastic form factor chosen as derivative of the optical potential

$$F(r) = \beta_2 R_V \frac{dV(r)}{dr} + i\beta_2 R_W \frac{dW(r)}{dr}$$

with $\beta_2 R_V = \beta_2 R_W = 1.21\ fm$ [11]. In Fig.1 the results of the calculations are compared with experimental data for the scattering of ^7Li. The geometric parameters of the optical potential were taken from the global parametrization [8], and the potential depths V and W were fitted (see table 1). From the calculations it follows that the contribution from inelastic processes is important except for very forward angles and that the experimental data can be described by usual optical potentials.

In the case of ^{11}Li the situation is different. The calculations based on the usual optical potentials cannot give a reasonable description of the experimental data. Fig.2 shows the elastic cross section of ^{11}Li calculated with the optical potential from the global parametrization [8]. The description of the experimental data can be obtained

only with an *anomalous* large value of surface diffuseness of the real part of the optical potential. The available experimental data for a rather narrow angle range only do not allow a detailed study of possible optical potential parameters. Therefore, only one example of possible potentials is given in Table 2. The corresponding elastic cross section, contribution from inelastic one, calculated in the same way as for the ^7Li case and the total cross section are shown in Fig. 2. As pointed out above, a striking peculiarity of the ^{11}Li optical potential (see table 2) is the unusual large value of surface diffuseness of the real part which apparently is a reflection of the "neutron" halo in the ^{11}Li density distribution. The r.m.s. radius of the real potential in this case is about 6 fm, and in the strong absorption region the potential has a refractive character. Further important information about the scattering nature may be obtained from a near-side/far-side decomposition of the elastic cross section [12]. The decomposition for the ^{11}Li elastic scattering is shown in Fig.3. The crossover point of the near-side and far-side components is close to $\theta \sim 2°$ and the region of diffractive oscillations occupies the angular range up to $\sim 8°$. At larger angles, the far-side component dominates the elastic cross section. In the case of ^7Li scattering the crossover point is near 8° and the region of diffractive oscillations spreads up to nearly 20°. The smoothness of σ/σ_R in the ^{11}Li case at angles larger than $\theta \geq 10°$ may be connected with a stronger manifestation of nuclear refractive properties in halo nuclei. The elastic cross section for the potential given in table 2 has characteristics of rainbow scattering [13]. Of course, it does not mean that clear rainbow scattering features are revealed in the ^{11}Li scattering: the appearance of this effect depends on the transparency of the nuclear potentials. For a more definite answer, it is necessary to have the experimental data for the ^{11}Li scattering in a wider angular interval, both the exponential fall-off of the elastic cross sections and the diffractive oscillations at small angles.

3 Microscopic approach to elastic proton scattering on nuclei in optical model

The description of nucleon elastic scattering on nuclei in the framework of the microscopic approach contains a large number of assumptions where at least some require a better justification from the first principles. In the intermediate-energy region ($E_p \geq$ 100 MeV) the description is somewhat simplified, implying a fewer approximations and a corresponding increase in the reliability of the theoretical analysis.

Therefore, we restrict ourselves to investigation of the elastic proton scattering on atomic nuclei at energies larger than 100 MeV. In this energy region the dynamics of the quasielastic process may be described as a single-step transition and the theoretical analysis is carried out in the framework of the distorted-wave impulse approximation (DWIA). The elastic scattering is defined by the optical potential which in the impulse approximation has two ingredients:

1. the structural information contained in the single-particle density distribution;
2. the effective interaction between the projectile and target nucleons.

In addition, it is necessary to take into account the identity of the nucleons in the collision partners which brings nonlocality to the reaction amplitude. For calculations of this amplitude, nonlocal densities would, in principle, be needed. The contribution of exchange knock-out amplitudes can, however, be approximated in the pseudopotential approach [14]. In that approximation, the nonlocal amplitude is reduced to a local one; hence, the local densities can be used in our cross section calculations.

The optical potential used for calculating elastic scattering was computed in a ρt-folding model [15] (in the following simply "folding-model") where ρ is the single-particle matter density of atomic nucleus. The central part of the optical potential was derived from the S=0, T=0 component of the NN forces. It is well known [16, 17] that, in this channel, there are essential corrections due to the influence of the nuclear medium which creates the ρ dependence of the effective NN forces. The ρ dependence of the effective forces was introduced in the evaluations of the optical potentials by a simple prescription suggested in ref.[16]. The spin-orbital part of the optical potential was evaluated without a ρ-dependent $(\vec{l} \bullet \vec{s})$ component of the t-matrix interaction. As an example, Fig.4 shows the comparison between experimental data (ref. [18]) and theoretical calculations for elastic proton scattering on ^6Li at E_p= 185 MeV. The dashed line corresponds to calculations with the t-matrix interaction describing the free NN scattering (ref.[15]) while the solid one takes into account medium effects. Our results correspond to microscopic calculations of elastic scattering with ingredients tested against weak and electromagnetic data as well as nucleon-induced quasielastic (p,p'), (n,p) and (p,n) on ^6Li as a target discussed in [6]. On the whole, we have reasonable agreement with experiment.

As far as the comparison between elastic cross sections on ^6Li and ^6He is concerned, the use of free NN interaction or other recipes for introducing the ρ dependence practically does not change the relative differences.

The single-particle matter densities of ^6He and ^6Li were calculated within the framework of the hyperspherical function method using the $\alpha + N + N$ model with conventional αN and NN potentials. The elements of the method and some results are outlined in Refs.[5, 6]. In Fig.5a the calculated matter densities of ^6Li and ^6He are shown. One may notice that ρ for ^6He is larger than for ^6Li for asymptotic values of r and, as a consequence, the opposite situation holds at smaller values of r.

The radial behavior of the calculated optical potentials changes systematically with increasing projectile energy: the real attractive part of the potential decreases and the repulsive core becomes bigger at higher energies. As an example, the optical potentials for protons at E_p=100 MeV are given in Fig.6. The difference in nuclear structure gives some changes in the optical potentials. As a consequence of a more loose structure at distances $r \geq 3$ fm, the absolute value of the ^6He potentials is greater than for ^6Li. And vice versa, at small r the core is somewhat more pronounced in the case of ^6Li.

In Fig.7 the resulting elastic cross sections are shown. At the very forward angles, the Coulomb interaction dominates and, naturally, the cross section on ^6Li is greater than on ^6He. At intermediate angles, the cross sections are close to each other. If we switch off the Coulomb interactions, theoretical cross sections for proton scattering on ^6Li and ^6He become very similar in this region of angles. At larger angles ($\theta \geq 20°$) the cross section on ^6Li is again greater than on ^6He and the difference between them

increases with scattering angle. Therefore, the differences in the structure of the target nuclei are displayed most clearly at large angles.

It is interesting to investigate the sensitivity of the elastic cross section to modifications of the densities. A cut-off of the density at $r \geq 4$ fm gives a negligible contribution to the elastic cross section while the region from 3 fm up 4 fm exerts some influence on the cross section at small angles. In Fig. 8a the real part of the potential for the p+^6He elastic scattering at E_p=100 MeV is compared with that calculated with densities cut at r=3 fm. In Fig. 8b the corresponding cross sections are shown. It is clear that the neglect of the outer part of the density modifies the potential surface, which is reflected mainly in the cross section form for angles $\theta \leq 20°$.

Fig.5b shows the contributions to the total densities from the α-particle core and outer nucleons. The outer nucleons in ^6Li and ^6He have different spatial distributions and correlations which influence the part of the single particle distribution of these nuclei determined by the α-particle. The total density at distances $r \leq 2.5$ fm is mainly determined by the nucleons of the core while at distances from 2.5 fm up to 3.5 fm it is determined both by the nucleons of the core and outer nucleons. The influence of the difference of the α-particle spatial distribution in ^6Li and ^6He due to different correlations of the outer nucleons in these nuclei can be displayed in the elastic scattering of protons on the α-particle core from ^6Li and ^6He. Fig.7d shows that the difference at large angles and the value of the effect is comparable with that at the scattering on Li and He.

As is seen, the process of elastic scattering at intermediate energies shows up some, although not pronounced, sensitivity to the correlation of the valence nucleons.

It is very interesting to estimate the elastic cross sections for proton scattering on ^{11}Li. For the ^{11}Li matter density we will use three different nuclear structure models. In the first, in the same spirit as for A = 6 nuclei, the hyperharmonic three-body model for ^{11}Li with ^9Li core is used. The second one (ref.[19]) is a simple three-body cluster oscillator shell model approximation (COSMA) with parameters fixed by ^{11}Li geometrical characteristics. The third one (ref.[20]) is a self-consistent shell model in the framework of the theory of finite-fermi systems. The potential of an average field and nucleon distributions are calculated by the density functional method. The resulting densities are presented in Fig.9a. The behavior of the density in the asymptotic region is different in all models reflecting different structures of the neutron halo. At small distances the most remarkable distinction is connected with the core and in the self-consistent shell model the density is lower as compared with the other calculations. But in the intermediate region (from $r \sim 2$ fm to ~ 4 fm) densities are similar for all models. The corresponding proton elastic cross sections for E_p= 100 MeV are given in Fig.9b. The meaningful distinctions are seen only at large angles, confirming the sensitivity to difference in the density behavior at small distances.

At last, we can state that in proton elastic scattering at intermediate energies it is difficult to comprehend the structure of neutron halo that must be revealed at small angles. But the influence of outer nucleons on the core can be investigated at large angles. As follows from our calculation, the studies of neutron halo effects have perspectives at lower energies where reactions become more peripheral and cross sections for the pn-scattering increase. As a consequence, the contribution from neutron halo reveals more clearly.

4 Elastic scattering in Glauber approach

It is well-known that a good description of the hadron-nucleus and nucleus- nucleus interactions has been obtained at high energies in the Glauber multiple-scattering theory [24]-[26]. Recently a reasonable description has also been achieved of nucleus-nucleus elastic scattering at 30 MeV/A and higher energies within the optical limit of the Glauber model [27]. This argues the Glauber approach to be a possible tool for investigating the halo structure of the exotic nuclei in the elastic scattering in the intermediate and lower energy region. We will here give main ingredients of the Glauber multiple-scattering theory and results obtained within this framework. Various approximations to this approach will also be briefly discussed.

One of the main points of the theory is the assumption of eikonalization of the elastic scattering amplitude

$$f(\theta) = \frac{i}{2k}\sum_l (2l+1)(1-e^{2i\chi_l})P_l(\cos\theta), \tag{1}$$

which means that a large number of partial waves contributes to the scattering amplitude. By assuming the scattering phase χ_l to be a nonsingular function of l, the sum can be replaced by an integral over $b = (l+\frac{1}{2})/k$

$$f(\theta) = \frac{ik}{2\pi}\int d^2b e^{i(\vec{q}\cdot\vec{b})}(1-e^{2i\chi(\vec{b})}), \tag{2}$$

b is the impact parameter, k the wave number of the incident particle, $\vec{q} = \vec{k} - \vec{k'}$ the wave vector transfer. The quantity $\gamma(\vec{b}) = 1 - e^{2i\chi(\vec{b})}$ is the so called profile function or the scattering amplitude in the impact parameter representation. It is connected with the interaction potential under the assumption of rectilinear propagation by the relationship

$$\gamma(\vec{b}) = 1 - \exp[-\frac{i}{\hbar v}\int_{-\infty}^{+\infty} V(\sqrt{b^2+z^2})dz]. \tag{3}$$

In the case of hadron-nucleus scattering, one has due to the potential additivity

$$\Gamma_{hA}(\vec{b}) = 1 - \exp\left[-\frac{i}{\hbar v}\sum_{j=1}^{A}\int_{-\infty}^{+\infty} V(\sqrt{(\vec{b}-\vec{s}_j)^2+(z-z_j)^2})dz\right], \tag{4}$$

where $(\vec{s}_j, z_j)$ are the j-th nucleon coordinates, A the mass number of the nucleus. One can rewrite the relationship (4) as follows:

$$\begin{aligned}\Gamma_{hA}(\vec{b}) &= 1 - \exp[2i\sum_{j=1}^{A}\chi(\vec{b}-\vec{s}_j)] = \\ &= 1 - \prod_{j=1}^{A}[1-\gamma(\vec{b}-\vec{s}_j)].\end{aligned} \tag{5}$$

The last expression does not contain the potential explicitly.

To describe the scattering of hadrons on the nucleus, equation (5) should be averaged over target nucleon positions, which gives

$$F_{hA}(\vec{q}) = \frac{ik}{2\pi}\int d^2b e^{i(\vec{q}\cdot\vec{b})}\{1-\prod_{j=1}^{A}[1-\gamma(\vec{b}-\vec{s}_j)]\} \mid \psi_A \mid^2 d^3r_1 \ldots d^3r_A. \tag{6}$$

Thus, the Glauber approximation is based on the following assumptions:

- rectilinear propagation of the hadron inside the nucleus
- additivity of phase shifts
- "freezing" of the motion of the nucleons in the nucleus

These assumptions while being well justified at high energies are questionable at intermediate ones. Nevertheless, we attempt to determine the applicability of this approach for the intermediate energies considering its straightforward generalization with minimal corrections.

First of all, the nuclear wave function has to be chosen. The simplest assumption for the wave function squared is an uncorrelated product of single-particle densities

$$\mid \psi_A \mid^2 = \prod_{j=1}^{A}\rho_A(\vec{s}_j, z_j). \tag{7}$$

Substituting (7) into (6) gives in the limit $A \to \infty$

$$\begin{aligned}F_{hA}(q) &= \frac{ik}{2\pi}\int d^2b e^{i(\vec{q}\cdot\vec{b})}\{1-[1-\int\gamma(\vec{b}-\vec{s})\rho_A(\vec{s},z)d^2sdz]^A\} \simeq \\ &\simeq \frac{ik}{2\pi}\int d^2b e^{i(\vec{q}\cdot\vec{b})}\{1-\exp[-A\int\gamma(\vec{b}-\vec{s})\rho_A(\vec{s},z)d^2sdz]\}.\end{aligned} \tag{8}$$

A more precise representation

$$\mid \psi_A \mid^2 = \delta(\sum_{j=1}^{A}\vec{r}_j/A)\prod_{j=1}^{A}\tilde{\rho}_A(\vec{s}_j, z_j) \tag{9}$$

gives

$$F_{hA}(q) = \frac{ik}{2\pi} K(\vec{q}) \int d^2b e^{i(\vec{q}\cdot\vec{b})} \{1 - \exp[-A \int \gamma(\vec{b}-\vec{s}) \tilde{\rho}_A(\vec{s},z) d^2s dz]\}. \quad (10)$$

The function $K(\vec{q})$ is called the center of the mass correlation factor. If $\tilde{\rho}_A = \frac{1}{(\pi R_A^2)^{3/2}} e^{-r^2/R_A^2}$, then

$$K(\vec{q}) = \exp(R_A^2 q^2/4A) \quad (11)$$

This factor has the same form in the oscillator model for the nucleus.

As is seen, $K(\vec{q}) \to 1$ for $A \to \infty$. The Glauber amplitude in this case coincides with the expression for the amplitude in the folding-model using the $t-$matrix of the free NN scattering. For finite nuclei it differs both by the factor $K(\vec{q})$ and the phase expression.

The "folding-model" uses the single particle density defined by

$$\rho_A(r) = \frac{1}{A} \sum_{i=1}^{A} \mid \psi_A \mid^2 d^3r_1 \dots d^3r_A \delta(\vec{r} - \vec{r}_i).$$

It has a Gaussian form for the parametrization (9)

$$\rho_A(\vec{r}) = \frac{1}{(\pi R_A^2 \frac{A-1}{A})^{3/2}} \exp[\frac{-r^2 A}{R_A^2 (A-1)}].$$

The Glauber approximation deals with the density $\tilde{\rho_A}$ describing a nuclear system as a more "loose" nucleus than the real one. Therefore the "folding-model" predicts the diffraction maxima and minima to be positioned at some greater angles than the Glauber approximation does. It also predicts a steeper decrease of the cross sections versus scattering angle due to absence of the $K(\vec{q})$ factor[1]. These differences can be minimized by introducing the matter corrections to the $t-$matrix or the effects of dynamic polarization. Both these corrections are strongly model-dependent. The Glauber approach gives, in this sense, a regular method for taking them into account.

In the calculations presented below, we use, for ^6He and ^6Li, proton and neutron distributions (ρ_A^p and ρ_A^n) calculated in [5, 6]. For ^{11}Li the self-consistent shell model density [20] was used. The squares of the wave functions were represented in the form (9) by fitting $\tilde{\rho}_A^p$ and $\tilde{\rho}_A^n$. It should be noted that in this representation nontrivial correlations of the halo neutrons have been lost. Their influence on the differential cross sections, as calculation shows, is small and does not affect the results. The ordinary nucleus ^{12}C was described in the oscillator model with the parameter obtained from the elastic formfactor data.

The second question is the choice of the reference frame. As is known, the Glauber approximation is nonrelativistic. Therefore, the choice of the frame is important. Usually, a center-of-mass-system is chosen. In this system the vector $\vec{q}$ can be defined

[1]It does not take place for nucleus-nucleus scattering (see below).

in a different way. If the z-axis is directed along the incident particle momentum $\vec{k}$, then $q = k \sin\theta$ where θ is the scattering angle. The best result is given, however, by choosing the Breit frame. In this frame $q = 2k \sin\theta/2$. This definition provides the simplest consideration of deviations from the rectilinear propagation of the incident particle. In all calculations we used the last definition of q.

The amplitudes of $pp-$ and $pn-$ interactions over the pion production threshold were parametrized in the form [28]

$$f_{NN}(q) = \frac{ik}{4\pi} \sigma_{NN}(1 - i\rho) e^{-aq^2}. \quad (12)$$

Below the threshold the amplitudes are assumed to be isotropic. The cross sections of the $pp-$ and $pn-$ interactions were calculated according to ref. [29]

Fig.10 shows the calculations of the elastic scattering differential cross sections of ^6He, ^6Li, ^{11}Li and ^{12}C nuclei on protons. As is seen, the Glauber model is in good agreement with the experimental data on $^{11}Li + p$ at $60MeV/A$. The description of $^6Li + p$ is of lesser quality. This may be due to the neglect of the Pauli principle and spin dependence of the $NN-$amplitude. A simplistic treatment of the Pauli principle [21] practically does not affect the cross section of the $^{11}Li + p$ but sizably decreases the cross section of the $^6Li + p$ both at small and large scattering angles. A correct inclusion of the Pauli principle requires much more details of the wave function and essentially complicates the calculations. Therefore, we restricted ourselves to this result at the present stage of investigation.

A larger difference between the cross sections for $^6He - ^6Li$ and $^{11}Li - ^{12}C$ at small angles at low energies is explained mainly by the difference of the $pp-$ and $pn-$ cross sections that at $60MeV$ is about $86mb$. Therefore, the presence of the neutron on the ^6He periphery instead of the proton in ^6Li is revealed already in the total cross sections. At higher energies, when the $pp-$ and $pn-$ cross sections practically coincide, the main differences in the cross sections for ^6He and ^6Li is due to slightly different nucleus sizes. A large difference of ^{11}Li and ^{12}C cross sections at large angles is due to the different density behavior of ^{11}Li and ^{12}C at small r.

In the large angular region, the order of distinction of the cross section $^6He - ^6Li$ and $^{11}Li - ^{12}C$ weekly depends on the energy and increases with the transferred momentum. Taking into account the small intensity of the radioactive beams, we find that just the experimental study of the elastic scattering of exotic nuclei at energies $60MeV/A$ and lower is of particular interest.

For nucleus-nucleus elastic scattering the amplitude is a straightforward generalization of that for hadron-nucleus scattering

$$F_{AB}(\vec{q}) = \frac{ik}{2\pi} \int d^2b e^{i(\vec{q}\cdot\vec{b})} \Gamma_{AB}(\vec{b}) = \quad (13)$$

$$= \frac{ik}{2\pi} \int d^2b e^{i(\vec{q}\cdot\vec{b})} d^3r_1 \dots d^3r_A d^3t_1 \dots d^3t_B, \mid \psi_A \mid^2 \mid \psi_B \mid^2 \times$$

$$\times \{1 - \prod_{j=1}^{A} \prod_{n=1}^{B} [1 - \gamma(\vec{b} - \vec{s}_j + \vec{\tau}_n)]\}. \quad (14)$$

Expression (14) can be simplified in the limit $A, B \to \infty$, $AB\sigma_{NN} \to const$

$$F_{AB}(\vec{q}) \simeq \frac{ik}{2\pi} K_A(\vec{q}) K_B(\vec{q}) \int d^2b e^{i(\vec{q}\cdot\vec{b})} \times$$
$$\{1 - [1 - \int d^3r d^3t \tilde{\rho}_A(\vec{r}) \tilde{\rho}_B(\vec{t}) \gamma(\vec{b} - \vec{s} + \vec{\tau})]^{AB}\} \simeq$$
$$\simeq \frac{ik}{2\pi} K_A(\vec{q}) K_B(\vec{q}) \int d^2b e^{i(\vec{q}\cdot\vec{b})} \times$$
$$\{1 - \exp[-AB \int d^3r d^3t \tilde{\rho}_A(\vec{r}) \tilde{\rho}_B(\vec{t}) \gamma(\vec{b} - \vec{s} + \vec{\tau})]\}. \quad (15)$$

Expression (15) is known as the Czyz-Maximon approximation [30]. An analog of the Czyz-Maximon approximation was used [31] in the analysis of data on high-energy inelastic reactions but led to unsatisfactory results. Theoretical corrections [32]-[34] to the approximation appeared to be so large that an alternative method for calculation of the scattering amplitude should be looked for. In particular, a "rigid projectile" approximation was suggested [35, 36]. This approximation considers the projectile as an "elementary" particle having no structure and characterized only by its scattering amplitude. The corresponding expression is

$$K_A(\vec{q}) K_B(\vec{q}) F_{AB}(\vec{q}) = \frac{ik}{2\pi} \int d^2b e^{i(\vec{q}\cdot\vec{b})} \{1 - \exp[-B \int d^3t \tilde{\rho}_B(\vec{t}) \Gamma_{NA}(\vec{b} + \vec{\tau})]\}. \quad (16)$$

This approximation improved the description of the data for interactions between light and heavy nuclei [37].

A regular method for the F_{AB} calculation was suggested in [38]-[41]. Briefly, it consists in the following [41]. The amplitude is expanded in a power series of the $NN-$interaction amplitude

$$\begin{aligned}
\Gamma_{AB}(\vec{b}) &= AB \int d^3r d^3t \tilde{\rho}_A(\vec{r}) \tilde{\rho}_B(\vec{t}) \gamma(\vec{b} - \vec{s} + \vec{\tau}) - \\
&- \frac{A(A-1)}{2!} B \int d^3r_1 d^3r_2 d^3t \tilde{\rho}_A(\vec{r}_1) \tilde{\rho}_A(\vec{r}_2) \tilde{\rho}_B(\vec{t}) \gamma(\vec{b} - \vec{s}_1 + \vec{\tau}) \gamma(\vec{b} - \vec{s}_2 + \vec{\tau}) - \\
&- A \frac{B(B-1)}{2!} \int d^3r d^3t_1 d^3t_2 \tilde{\rho}_A(\vec{r}) \tilde{\rho}_B(\vec{t}_1) \tilde{\rho}_B(\vec{t}_2) \gamma(\vec{b} - \vec{s} + \vec{\tau}_1) \gamma(\vec{b} - \vec{s} + \vec{\tau}_2) \\
&- \frac{A(A-1)B(B-1)}{2!2!} \left[\int d^3r d^3t \tilde{\rho}_A(\vec{r}) \tilde{\rho}_B(\vec{t}) \gamma(\vec{b} - \vec{s} + \vec{\tau}) \right]^2 + \ldots \quad (17)
\end{aligned}$$

At large A and B the binomial coefficients can be written as $C_A^k \simeq A^k/k!$, $k \ll A$. The series (17) then reduces to the exponential expression

$$\begin{aligned}
\Gamma_{AB}(\vec{b}) &= 1 - \exp\left\{ -AB \tilde{\rho}_A \otimes \tilde{\rho}_B \otimes \gamma + \frac{AB^2}{2!} \tilde{\rho}_A \otimes \tilde{\rho}_B \otimes \tilde{\rho}_B \otimes \gamma \otimes \gamma + \right. \\
&+ \frac{A^2 B}{2!} \tilde{\rho}_A \otimes \tilde{\rho}_A \otimes \tilde{\rho}_B \otimes \gamma \otimes \gamma + \\
&+ \left. \frac{A^2 B^2}{2!2!} [\tilde{\rho}_A \otimes \tilde{\rho}_B \otimes \gamma]^2 + \ldots \right\} \quad (18)
\end{aligned}$$

The first term in the exponential gives the Czyz-Maximon expression. Gathering the terms of the first order in B, one obtains the "rigid projectile" approximation. Finally, retaining all the leading terms in (17) gives [40]

$$\Gamma_{AB}(\vec{b}) = 1 - \exp[-\Phi(\vec{b})] \quad (19)$$

$$\begin{aligned}
\Phi(\vec{b}) &= \frac{2}{\sigma_{NN}} \int d^2s [x + y - u - z - uz] \\
x &= \frac{\sigma_{NN}}{2} A \int_{-\infty}^{+\infty} \tilde{\rho}_A(\sqrt{\vec{s}^2 + z^2}) dz, \\
y &= \frac{\sigma_{NN}}{2} B \int_{-\infty}^{+\infty} \tilde{\rho}_B(\sqrt{(\vec{b} - \vec{s})^2 + z^2}) dz,
\end{aligned} \quad (20)$$

u and z are solutions of the system of transcendental equations

$$\begin{cases} u = ye^{-z} \\ z = xe^{-u}. \end{cases} \quad (21)$$

This approximation is called the "tree" approximation because terms of the series (17) retained in (20) are represented by bicolored (bipartite) tree graphs [41].

Unfortunately, these approaches encounter a number of difficulties when investigating scattering of the neutron halo nuclei which have essentially different proton and neutron distributions. The first difficulty is the determination of the center of the mass correlation factor for nongaussian densities. One may only hope that the factor $K(\vec{q})$ of the form (11) for a reasonable choice of R_A would describe even such exotic densities but specific recipes are absent. Another problem is more serious. The phase function of elastic scattering in the Czyz-Maximon approximation is proportional to the nuclear single-particle densities. Therefore, a natural generalization would be

$$\begin{aligned}
\chi^{CM}(\vec{b}) &= -\frac{1}{2i} \{ \int d^2s d^2\tau \gamma_{pp}(\vec{b} - \vec{s} + \vec{\tau}) [Z_A \tilde{\rho}_A^p(\vec{s}) Z_B \tilde{\rho}_B^p(\vec{\tau}) + N_A \tilde{\rho}_A^n(\vec{s}) N_B \tilde{\rho}_B^n(\vec{\tau})] + \\
&+ \gamma_{pn}(\vec{b} - \vec{s} + \vec{\tau}) [Z_A \tilde{\rho}_A^p(\vec{s}) N_B \tilde{\rho}_B^n(\vec{\tau}) + N_A \tilde{\rho}_A^n(\vec{s}) Z_B \tilde{\rho}_B^p(\vec{\tau})] \}.
\end{aligned}$$

Here $Z_A, N_A (Z_B, N_B)$ are the charge and the neutron number of the nucleus $A(B)$, $\tilde{\rho}_A^p(\tilde{\rho}_B^p)$ and $\tilde{\rho}_A^n(\tilde{\rho}_B^n)$ are the corresponding single-particle densities. With this definition, however, a question about the correctness of the transition to the optical limit, separately for the protons and neutrons, arises. Finite-mass-number corrections to the Czyz-Maximon approximation can, in principle, be calculated in the tree approximation, but taking into consideration different densities essentially complicates the final expressions. Moreover, the increase of $Ref_{NN}(0)/Imf_{NN}(0)$ with decreasing energy requires calculation of numerous corrections to the tree phase function (20).

To avoid these problems, we use a method suggested in paper [42]. This method consists in the direct Monte Carlo evaluation of the multiple integrals of the Glauber theory. The nucleus-nucleus profile function $\Gamma_{AB}(\vec{b})$ is calculated in this approach as the mean value over the ensemble Ω_M of M sets of the nucleon coordinates

$$\Omega_M = \{\{\vec{r}_j\}_{j=1}^{A}, \{\vec{t}_n\}_{n=1}^{B}\}_{i=1}^{M}$$

distributed according to their densities and is given by the expression

$$\Gamma_{AB}(\vec{b}) \simeq \frac{1}{M} \sum_{\{\vec{r}\},\{\vec{t}\}\in\Omega_M} \{1 - \prod_{j=1}^{A}\prod_{n=1}^{B}[1 - \gamma(\vec{b} - \vec{s}_j + \vec{\tau}_k)]\}. \quad (22)$$

The method, in principle, allows arbitrary parametrization of γ_{NN} and $\tilde{\rho}_A, \tilde{\rho}_B$. As has been said previously, in particular calculations we used either the gaussian parametrization of γ_{NN} or the isotropic one

$$\gamma_{NN}(\vec{b}) = \frac{\sigma_{NN}^{tot}(2k_{NN}^{*})^2}{4\pi}\left(1 - i\frac{Ref_{NN}(0)}{Imf_{NN}(0)}\right)\frac{J_1(2k_{NN}^{*}b)}{2k_{NN}^{*}b}, \quad (23)$$

where k_{NN}^{*} is the nucleon wave number in the NN center-of-mass system. We defined the value of M from the stability condition of the calculated results in the region of the second diffraction maximum at twice increasing M. In the real calculation, M varied from 10^3 to 10^5 depending on the energy and projectile-target combination.

To compare the results obtained in various approaches, we have calculated differential elastic cross sections for nucleus-nucleus scattering at several energies and projectile-target combinations.

In Fig.11 calculations of the differential elastic cross sections for the $^4He+^{12}C$ reaction at energy $342MeV/A$ are shown. It is seen (Fig.11a) that the Czyz-Maximon approximation overestimates the cross section and gives incorrect positions of the diffraction minima and maxima. The folding-model, Czyz-Maximon approximation without taking into account $K(\vec{q})$, gives a better result. The description can be improved by a tuning of the nuclear density, as was done in [27], but the success for a more correct approximation is not guaranteed in this case. More substantiated "rigid projectile" and tree approximations give, at the same time, reasonable results without neglecting the center-of-mass correlations (Fig.11b). Taking into account corrections for the finiteness of the mass numbers of colliding nuclei, the radii of $NN-$interactions, etc. can improve these results (see, i.e., [40]).

Summarizing the results presented, we conclude that various approximations to the Glauber theory give close results in the region of the first diffraction maximum. At large scattering angles, various approaches give different results.

Similar conclusions can be drawn from the calculations of the $^{12}C+^{12}C$ scattering at various energies (Fig.12). In addition, we notice an increase in the accuracy of the predictions of the Czyz-Maximon approximation (with the center of mass correlation disregarded). Unfortunately, an increase in statistical errors hampers the direct Monte-Carlo evaluation of the cross section at an energy $30MeV/A$ beyond the first diffraction minimum and ambiguities of the solution of (21) prevent us from presenting the tree approximation and Monte-Carlo results. Therefore, the applicability of the Glauber theory at such low energies requires further investigations.

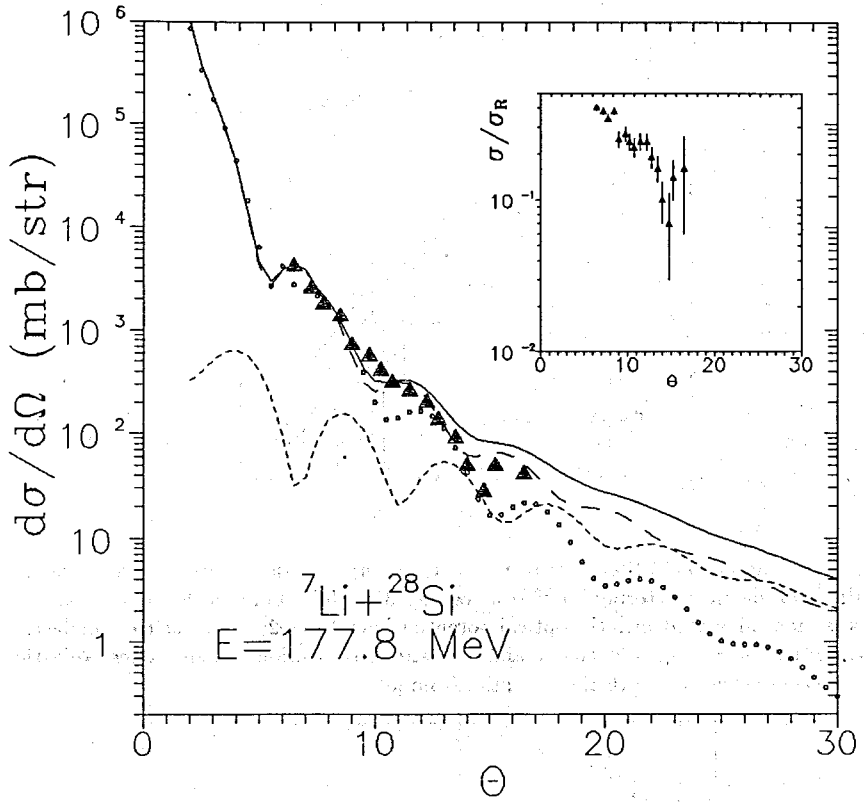

Fig. 1 Comparison of the experimental data (triangles) with the theoretical calculations for the ^7Li scattering on ^{28}Si at the energy 177.8 MeV. Long-dashed line – elastic cross section calculated with the optical potential from Table 1; short-dashed – inelastic cross section; solid – sum of elastic and inelastic cross sections; open circles – elastic cross section calculated with the potential from [8].

Table 1. Parameters of the optical potentials for $^7Li+^{28}Si$ at $29MeV/A$

N	V	R_R	a_R	W	R_I	a_I	$<r_R^2>^{1/2}$	$<r_I^2>^{1/2}$	σ_R	χ^2/N
C	226.75	1.286	0.853	37.26	1.739	0.809	4.38	5.08	1820.	7.0
[8]	114.2	1.286	0.853	29.75	1.739	0.809	4.38	5.08	1700.	10.4

Table 2. Parameters of the optical potential for $^{11}Li+^{28}Si$

V	R_R	a_R	W	R_I	a_I	$<r_R^2>^{1/2}$	$<r_I^2>^{1/2}$	σ_R	χ^2/N
204.48	0.585	1.737	8.23	2.18	0.425	6.604	5.36	1445.2	1.84

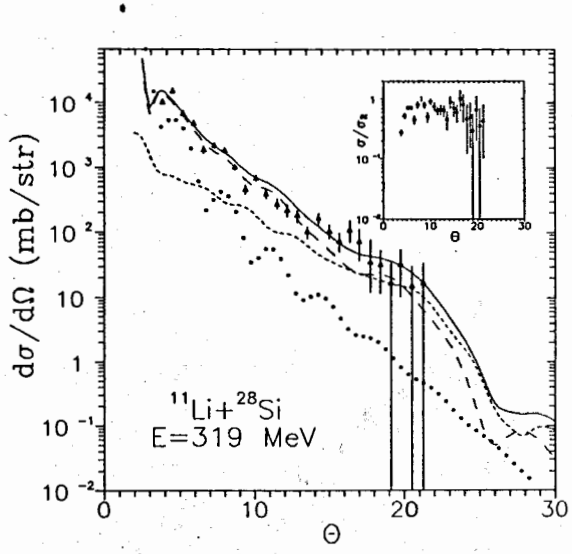

Fig. 2 Comparison of the experimental data (dots) with the theoretical calculations for the ^{11}Li elastic scattering on ^{28}Si at energy 319 MeV. Long-dashed line – elastic cross section calculated with the optical potential from Table 2; short-dashed – inelastic cross section; solid – sum of elastic and inelastic cross sections; open circles – elastic cross section calculated with the potential from [8].

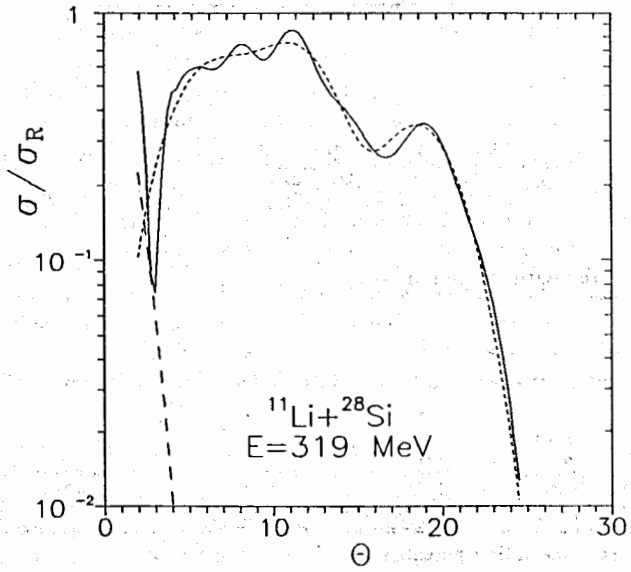

Fig. 3 The near-side/far-side decomposition of the elastic scattering ^{11}Li+^{28}Si at the energy 319 MeV. Solid line, long-dashed and short-dashed are elastic cross section, near-side and far-side contributions, respectively.

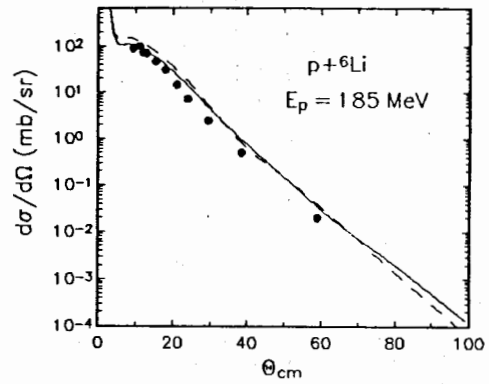

Fig.4 Comparison between theoretical proton elastic cross sections on ^6Li at E_p= 185 MeV and experimental data(ref. [40]). Calculation with free NN-interaction is shown by dashed line and with density dependence taken into account – solid line.

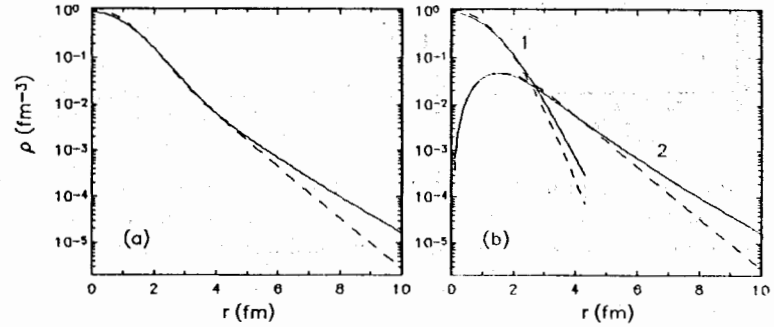

Fig.5 Densities in r space for ^6He (solid line) and ^6Li (dashed line); a) the total material and b) the contributions to the total densities from the α-particles (curves 1) and outer nucleons (curves 2). All densities are normalized as $\int dr r^2 \rho(r) = A/\sqrt{4\pi}$.

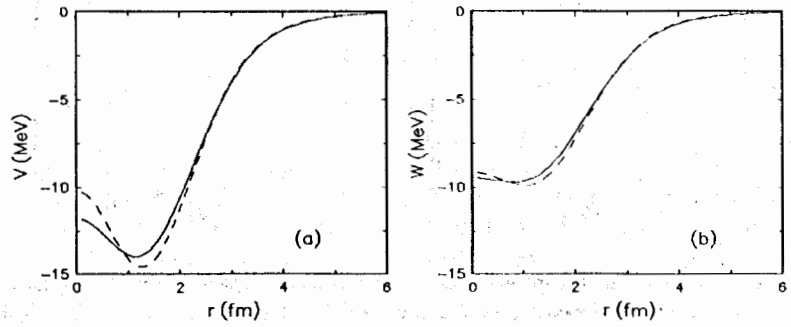

Fig.6 Real (a) and imaginary (b) parts of the optical potential for proton elastic scattering on ^6He (solid line) and ^6Li (dashed line) at E_p=100 MeV.

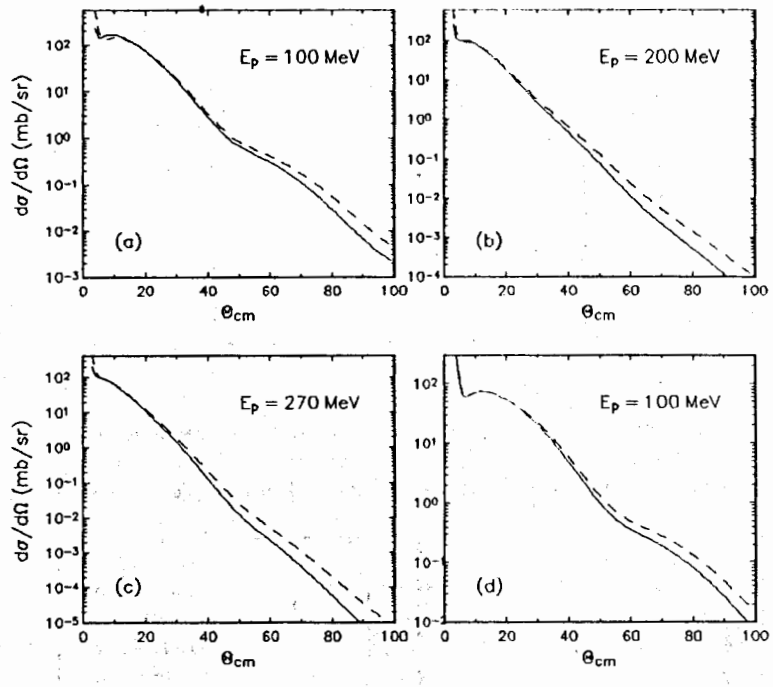

Fig.7 Proton elastic cross sections on ^6He (solid line) and ^6Li (dashed line) at the energies a) 100 MeV; b) 200 MeV; c) 270 MeV. Part d) shows proton cross sections for scattering on α-core in ^6He (solid line) and ^6Li (dashed line) at E_p=100 MeV.

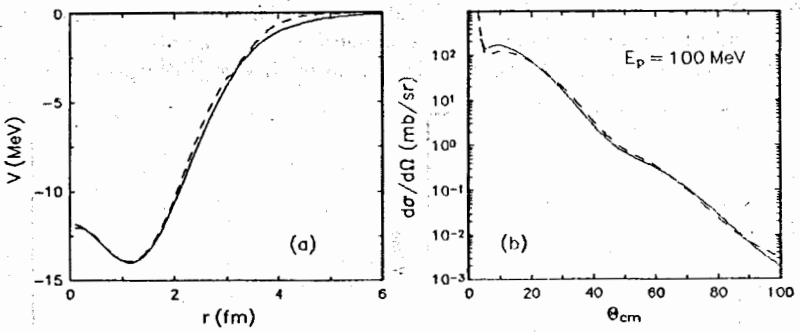

Fig.8 a) Real parts of the optical potential for proton scattering on ^6He at E_p=100 MeV, calculated with full density (solid line) and for density cut at r=3 fm (dashed line); b) the corresponding elastic cross sections.

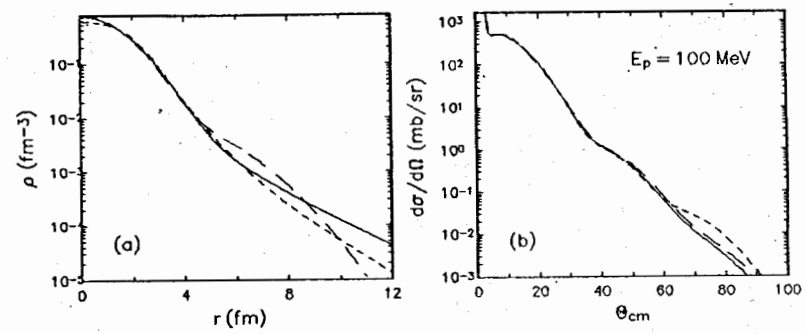

Fig.9 a) Total matter densities in r space for ^{11}Li. Solid line – hyperharmonic three-body model, long dashed – "COSMA" model, short dashed – model [20]; b) corresponding proton elastic cross sections at E_p= 100 MeV.

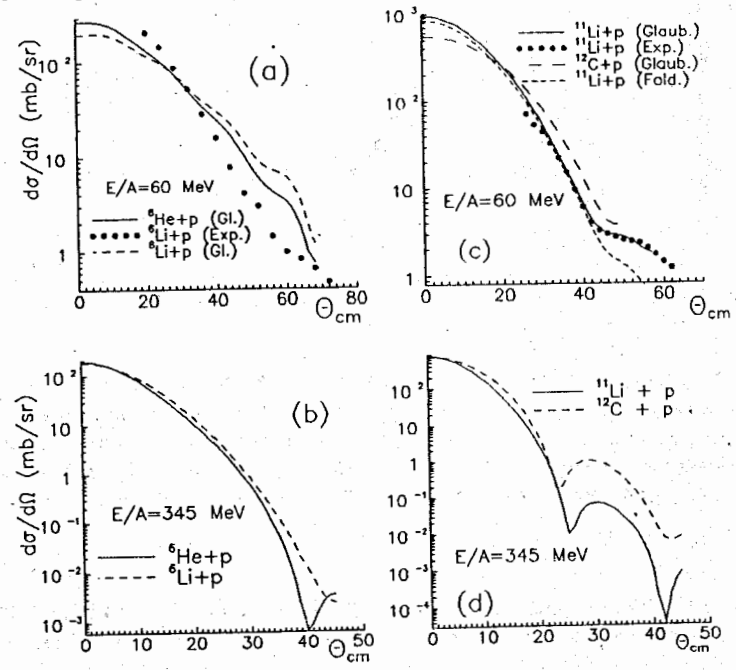

Fig.10 a) The differential elastic cross sections for ^6He+p, ^6Li+p reactions at $60MeV/A$. The solid line corresponds to the ^6He+p case, the dashed one – ^6Li+p. The points – the experimental data for ^6Li+p [2]; b) The differential elastic cross sections for ^6He+p, ^6Li+p reactions at $345MeV/A$. The solid line corresponds ^6He+p, the dashed one – ^6Li+p. c) The differential elastic cross sections for $^{11}Li+p$, $^{12}C+p$ reactions at $60MeV/A$. The solid line corresponds $^{11}Li+p$, the short dashed one – "folding" approximation. The long dashes – $^{12}C+p$. The points are the experimental data on $^{11}Li+p$ [2] d) The differential elastic cross sections for $^{11}Li+p$, $^{12}C+p$ reactions at $345MeV/A$. The solid line corresponds $^{11}Li+p$, the dashed one – $^{12}C+p$ reactions.

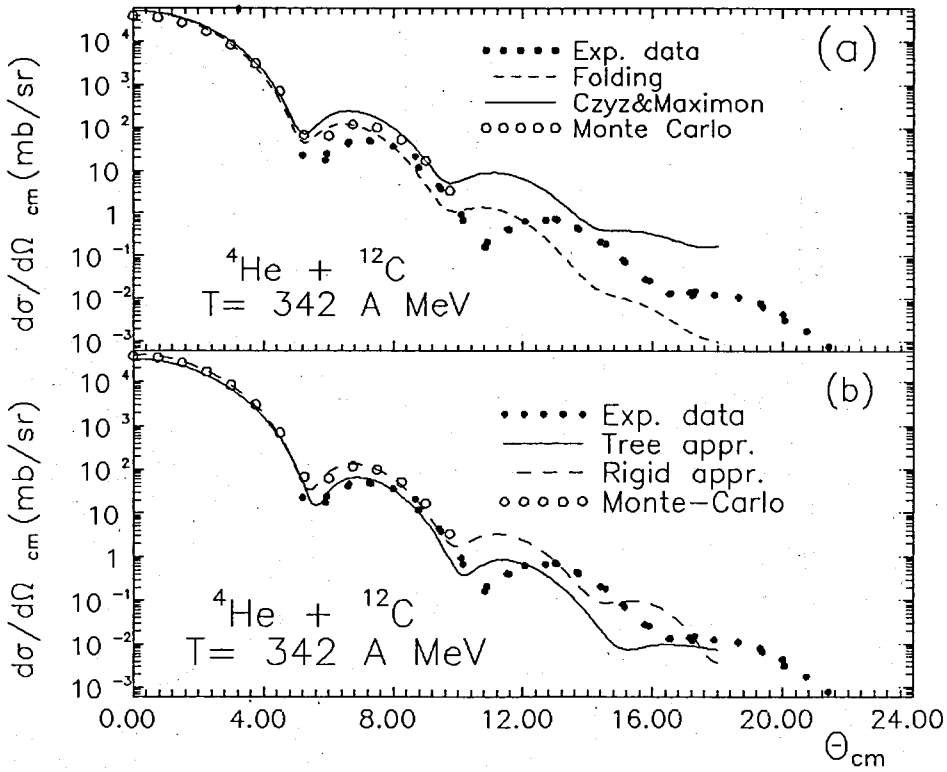

Fig.11 The differential elastic cross sections for $^4He+^{12}C$ reactions at $342MeV/A$ within the framework of various approximations to the Glauber theory: a)the "folding" approximation (dashed line), the Czyz-Maximon approximation (solid line), the Monte-Carlo results (open circles), the experimental data [37](points); b)the tree approximation (solid line), the "rigid projectile" approximation (dashed line),the Monte-Carlo results (open circles), the experimental data [37] (points).

In Fig.13 the Monte-Carlo calculations of the elastic scattering of the nuclei ^6He, ^6Li, ^{11}Li and ^{12}C on the nucleus ^{12}C are presented. The picture looks like the one of scattering on hydrogen but less distinct; at low energies one can expect a total cross section difference to be of an order of $\sim 10\%$ in comparison with $\sim 30\%$ for the scattering on hydrogen. The differences in the large-angle region are greater for the ^{11}Li and ^{12}C scattering (Fig.13b,d). Thus, for investigation of geometrical characteristics of halo nuclei, experiments at low energies on the hydrogen target are preferable.

As is seen, the theoretical analysis of elastic scattering in the first-diffraction-maximum region is relatively model-independent and can be carried out practically without free parameters. Therefore, the elastic scattering data on exotic nuclei and the corresponding Glauber-like approaches can be considered an effective tool for studying the neutron halo structure.

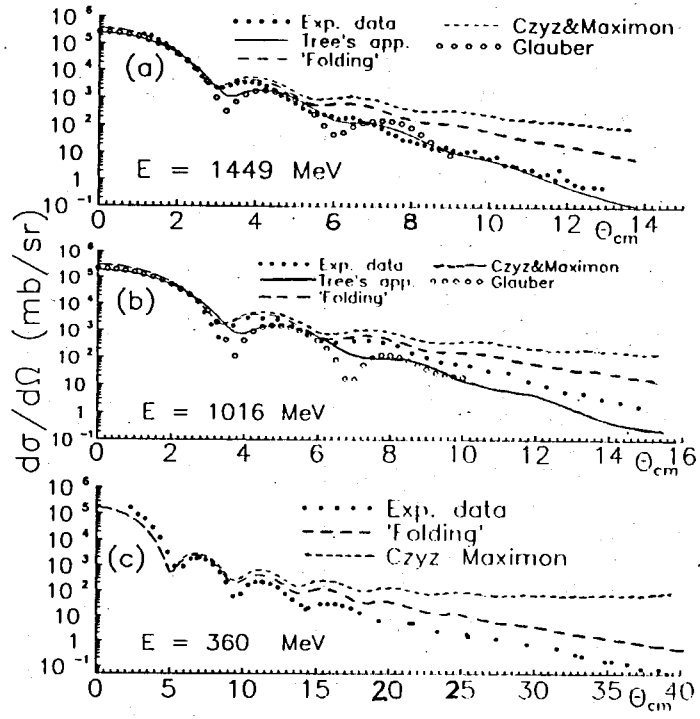

Fig.12 The differential elastic cross sections for $^{12}C+^{12}C$ reactions at various energies (pointed in the pictures) within the framework of various approximations to the Glauber theory: the 'folding' approximation (long dashes), the Czyz-Maximon approximation (short dashes), the Monte-Carlo results (open circles), the experimental data [43] (full circles), the tree approximation (solid line).

At higher transferred momenta theoretical uncertainties are larger. The reason for the discrepancy may be both uncertainties of the approximations to the Glauber theory and drawbacks of the Glauber approach itself. The results of the direct evaluation of the Glauber expressions, using the Monte-Carlo method [42], show that for correct description of the data the Glauber approach should be modified. The most important correction due to the deviation from the eikonal propagation could be taken into account by using the optical potential reconstructed from the Glauber phase shifts [25]

$$U_{opt}(r) = \frac{\hbar v}{\pi r}\frac{d}{dr}\int_r^{+\infty} bdb\frac{\chi_{opt}(b)}{\sqrt{b^2-r^2}}, \qquad (24)$$

which can be used in the conventional distorted wave approximation by properly taking into account the distortions in the relative motion of colliding nuclei due to the Coulomb+nuclear forces [27, 44]. Nevertheless, our preliminary results in the standard Glauber approach seem to be very promising in describing both the absolute value and the functional dependence of elastic scattering without free parameters.

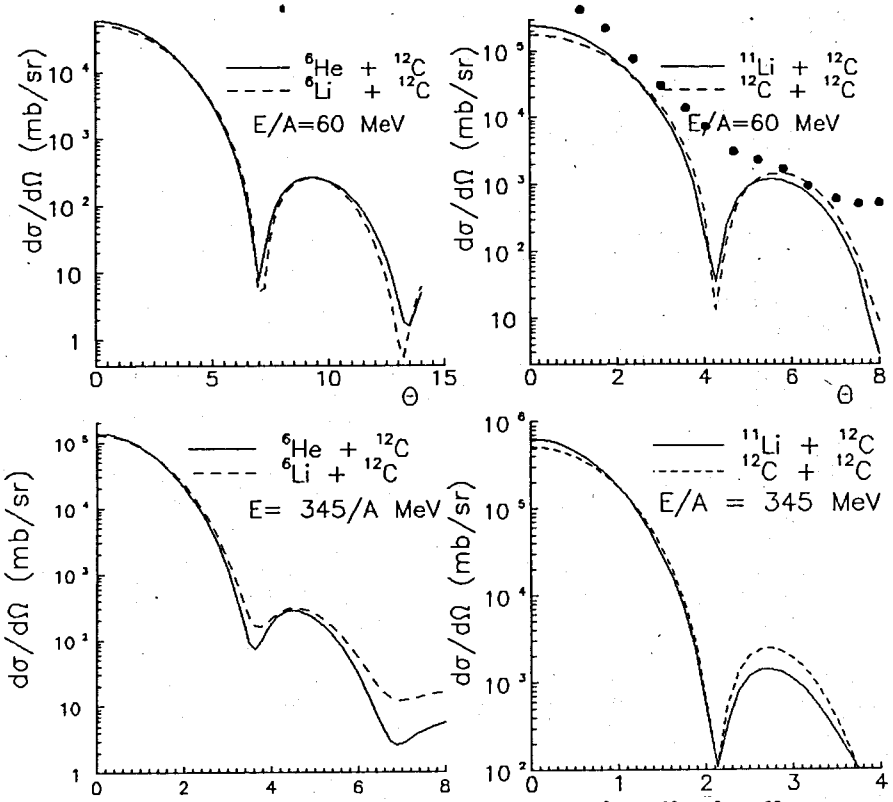

Fig.13 a) The differential elastic cross sections for ^{6}He+^{12}C, ^{6}Li+^{12}C reactions at $60MeV/n$. The solid line corresponds to ^{6}He+^{12}C; the dashed one, to ^{6}Li+^{12}C. b) The differential elastic cross sections for ^{6}He+^{12}C, ^{6}Li+^{12}C reactions at $345MeV/A$. The solid line corresponds to ^{6}He+^{12}C; the dashed one, to ^{6}Li+^{12}C. c) The differential elastic cross sections for ^{11}Li+^{12}C, ^{12}C+^{12}C reactions at $60MeV/A$. The solid line corresponds to ^{11}Li+^{12}C; the dashed one, to ^{12}C+^{12}C. The points are the experimental data [45] for ^{11}Li+^{12}C; d) The differential elastic cross sections for ^{11}Li+^{12}C, ^{12}C+^{12}C reactions at $345MeV/A$. The solid line corresponds to ^{11}Li+^{12}C; the dashed one, to ^{12}C+^{12}C reactions.

5 Conclusions

In the present paper we display very preliminary results in the description of elastic scattering of exotic nuclei in various approximations. As we have demonstrated, the elastic scattering will be able, in principle, to give the accurate information about integral properties of the neutron halo structure. Both theoretical and experimental investigations of the subject considered are in the very beginning and a further systematic study is desirable.

We thank J.S.Vaagen for a critical reading of the manuscript and stimulating discussion of the problem. We are also grateful to J.S.Vaagen, B.V.Danilin, S.A.Fayans, D.V.Fedorov and M.V.Zhukov for useful discussion.

References

[1] T. Kobayashi, em Nucl. Phys. **A538** (1992) 343.

[2] C. B. Moon et al., Preprint Riken-AF-NP-126, 1992.

[3] M. Lewitowich et al., in Proceedings of the International Conference on Exotic Nuclei, Crimea, 1-5 October 1991; preprint GANIL P 92 20, CAEN, 1992.

[4] H. Lenske, in Proceedings of the International Workshop on Gross Properties of Nuclei and Nuclear Excitations, Hirschegg, Austria, January 21-26, 1991, p.44.

[5] B. V. Danilin, M. V. Zhukov, L. V. Chulkov, A. A. Korsheninnikov and V. D. Efros, *Yad.Fiz.* **49** (1989) 351 *Sov. J. Nucl. Phys.* **49** (1989) 217; **49** (1989) 360 **49** (1989) 223.

[6] B. V. Danilin, M. V. Zhukov, S. N. Ershov, F. A. Gareev, J. S. Vaagen and J. M. Bang, *Phys. Rev.* **C43** (1991) 2835.

[7] R. Anne et al. *Phys. Lett.* **B250** (1990) 19.

[8] J. Cook, *Nucl. Phys.* **A388** (1982) 153.

[9] A. Nadasen et al., *Phys.Rev.* **C39** (1989) 536; **C40** (1989) 1237.

[10] M. S. Zisman et al., *Phys. Rev.* **C21** (1980) 2398.

[11] A. Nadasen et al., *Phys. Rev.* **C39** (1989) 536; *Phys. Rev.* **C40** (1989) 1237.

[12] R. C. Fuller, *Phys. Rev.* **C12** (1975) 1561.

[13] A. S. Dem'yanova et al., *Nucl. Phys.* **A501** (1989) 336.

[14] F. Petrovich et al., *Phys. Rev. Lett.* **22** (1969) 895; W. G. Love, *Nucl. Phys.* **A312** (1978) 160.

[15] M. A. Franey and W. G. Love, *Phys. Rev.* **C31** (1985) 488.

[16] J. J. Kelly, *AIP Conf.Proc.* No.**97**, edited by Hans-Otto Meyer (AIP, New York, 1982).

[17] F. A. Brieva and J. R. Rook, *Nucl. Phys.* **A296** (1978) 206; K. Nakayama and W. G. Love, *Phys. Rev.* **C38** (1988) 51.

[18] R. M. Hutcheon, O. Sundberg and G. Tibell, *Nucl. Phys.* **A154** (1970) 261.

[19] M.V. Zhukov, D.V. Fedorov, B.V. Danilin, J.S. Vaagen and J. Bang, *Nucl. Phys.* **A529** (1991) 53.

[20] S. A. Fayans, *ZhETF Pis'ma* **53** (1991) 389; *Phys. Lett.* **B267** (1991) 443. J.M.Bang, *Phys. Rev.* **C44** (1991) R12.

[21] A. N. F. Aleixo, C. A. Bertulani and M. S. Hussein, *Phys. Rev.* **C43** (1991) 2722.

[22] C. M. Perey and F. G. Perey, *Atomic Data and Nuclear Data Tables*, **17** (1976) 1.

[23] J. M. Bang, F. A. Gareev, W. T. Pinkston and J. S. Vaagen, *Phys. Rep.* **125** (1985) 253.

[24] A. G. Sitenko, *Ukrain. Fis. Journ.* **4** (1957) 152.

[25] R. J. Glauber, In: Lectures in Theoretical Physics, Ed. W. E. Brittin et al **1** (1959) N. Y.

[26] R. J. Glauber, Proc. of the 2nd Int. Conf. on High Energy Physics and Nuclear structure, (Rehovoth, 1967) Ed. G. A. Alexander, North-Holland, Amsterdam, 1867.

[27] S. M. Lenzi, F. Zardi and A. Vitturi, *Phys. Rev.* **C38** (1988) 2086; **C40** (1989) 2114; *Nucl. Phys.* **A536** (1992)168.

[28] R. D. Dolliver, F. Turtschi, *Ann. of Phys. (N.Y.)* **124** (1980) 124.

[29] S. K. Charagi, S. K. Gupta, *Phys. Rev.* **C41** (1990) 1610

[30] W. Czyz, L. C. Maximon *Ann. of Phys. (N.Y.)* **52** (1969) 59.

[31] J. P. Vary *Phys. Rev. Lett.* **40** (1978) 295.

[32] G. Fäldt, H. Pilkuhn, H. G. Schlaide *Ann. of Phys. (N.Y.)* **82** (1974) 326.

[33] Z. Kirzon, A. Dar *Nucl. Phys.* **A237** (1975) 319

[34] V. Franco, G.K. Varma *Phys. Rev.* **C18** (1978) 349.

[35] G. D. Alkhazov et al. preprint LNPI **465,473** Leningrad (1979)

[36] V. S. Barashenkov, G. G. Musulmanbekov *Acta. Phys. Pol.* **B10** (1979) 373.

[37] G. D. Alkhazov et al. *Nucl. Phys.* **A280** (1977) 365.

[38] I. V. Andreev *preprint FIAN* **92** Moscow (1976)

[39] I. V. Andreev, A. V. Chernov *Yad. Fiz.* **28** (1978) 477.

[40] A. S. Pak, A. V. Tarasov, V. V. Uzhinski and Ch. Cheren, *Pis'ma ZHETF* **28** (1978) 314; *Yad. Fiz.* **30** (1979) 102.

[41] V.V.Uzhinski *preprint JINR* **P2-81-789** Dubna (1981)

[42] S. Yu. Shmakov, V. V. Uzhinski and A. M. Zadorozhny, *Comp. Phys. Commun.* **54** (1989) 125.

[43] M. Buenerd *Nucl. Phys.* **A424** 1984 313.

[44] K. Yabana, Y. Ogava, Y. Suzuki *Nucl. Phys.* **A539** (1992) 295.

[45] J.J. Kolata et al. "Elastic scattering of ^{11}Li and ^{11}C from ^{12}C at 60 *MeV/nucleon*", *preprint MSU* (1992).

Received by Publishing Department
on November 13, 1992.